ARTICLE

High-Performance Biosensing Using Arrays of Plasmonic Nanotubes

John McPhillips,[†,*] Antony Murphy,[†] Magnus P. Jonsson,[‡] William R. Hendren,[†] Ronald Atkinson,[†] Fredrik Höök,[‡] Anatoly V. Zayats,[†] and Robert J. Pollard[†]

[†]Centre for Nanostructured Media, IRCEP, Queen's University of Belfast, BT7 1NN, United Kingdom, and [‡]Division of Biological Physics, Department of Applied Physics, Chalmers University of Technology, Sweden

ABSTRACT We show that aligned gold nanotube arrays capable of supporting plasmonic resonances can be used as high performance refractive index sensors in biomolecular binding reactions. A methodology to examine the sensing ability of the inside and outside walls of the nanotube structures is presented. The sensitivity of the plasmonic nanotubes is found to increase as the nanotube walls are exposed, and the sensing characteristic of the inside and outside walls is shown to be different. Finite element simulations showed good qualitative agreement with the observed behavior. Free standing gold nanotubes displayed bulk sensitivities in the region of 250 nm per refractive index unit and a signal-to-noise ratio better than 1000 upon protein binding which is highly competitive with state-of-the-art label-free sensors.

KEYWORDS: gold nanotubes · array · LSPR · label-free biosensing · plasmonic · metamaterial · finite element simulation

Biosensors are essential in areas such as disease diagnostics, environmental monitoring, and food safety and are also vital tools in the investigation of biological phenomena. Fluorescence-based methods have proven useful, for example, in both genomic and proteomic microarray-based analyses[1,2] and for imaging, including single molecule detection inside living cells.[3,4] However, labeling molecules with fluorophores can be expensive and time-consuming, and for certain applications it may not even be feasible. In addition, biological reactions in general rely on the three-dimensional structure of the biomolecules which may be affected by the addition of a fluorescent marker. Therefore, there has been a drive for bioanalytical sensor techniques that do not require labeling, but instead detect the target molecules directly. The transduction mechanism can be mechanical, such as in the quartz crystal microbalance with dissipation monitoring (QCM-D) that monitors changes in resonance frequency and damping of a piezoelectric oscillator during, for example, adsorption of biomolecules.[5,6] A nanowire field-effect sensor instead detects changes in conductivity on the sensor, which can be measured electrically.[7] The third main transducer principle is optical, where surface plasmon resonance (SPR) is one of the most commonly used methods today.[8] Here, changes in the refractive index (RI) near a flat metal surface are monitored optically by probing changes in the surface plasmon resonance (surface plasmons are collective oscillations of the free electrons near the metal interface).

In conventional SPR, light needs to couple to surface plasmon polaritons using prisms (Kretschmann configuration).[9] In contrast, in nanostructured metal films and metal nanoparticles, plasmon resonances can be excited by direct illumination without any special arrangements and measured using conventional transmission-mode spectroscopy.[10,11] This significantly simplifies the experimental setup, which is one of the reasons for the increasing popularity of nanoplasmonic biosensors. The optical properties of metallic nanoparticles are governed by localized surface plasmon resonances (LSPRs) which are displayed as, for example, peaks in an extinction spectrum (extinction $= -\ln$(transmission)). The LSPR position in the wavelength is sensitive to changes in RI in close proximity to the metal.[10]

A biomolecular recognition reaction of, for example, antigens binding to antibodies immobilized on the sensor surface can then be probed in real-time by monitoring shifts in the extinction peak wavelength. This suggests that the performance can be improved by increasing the sensitivity of the plasmonic resonance to changes in RI near the metal surface. This has been stud-

*Address correspondence to j.mcphillips@qub.ac.uk.

Received for review November 9, 2009 and accepted February 24, 2010.

Published online March 10, 2010. 10.1021/nn9015828

ied, for example, by varying both the shape of the nanostructure and also the material or type of support.[12−14] Further, to optimize the signal-to-noise ratio, which ultimately determines the lowest concentration of an analyte that is measurable, it is crucial to keep the noise level at a minimum. For LSPR sensors this means maximizing the precision with which the plasmonic resonance can be probed in real-time. For example, the peak position of a sharp peak might be monitored with better precision than a peak with large peak width. Further, it has been shown that monitoring the centroid of the peak (wavelength at the center of mass of the peak) can reduce the noise level significantly.[15]

From a practical as well as commercial point of view it is valuable to use low-cost and scalable fabrication methods. Therefore, several techniques that enable parallel fabrication of surface-supported plasmonic nanostructures have been developed, including nanosphere lithography,[16] sparse colloidal lithography,[17] hole-mask lithography,[18] and nanoimprint lithography.[19] Another promising approach is to use thin substrate-supported porous alumina as a template for electrodeposition of metals.[20] This method allows a wide range of nanostructures to be produced in a relatively simple fashion, such as both released and freestanding nanorods of different materials, including segmented[21] and coaxial structures.[22−24]

While the refractive index sensing capability of many plasmonic nanostructures has been reported,[25−31] to our knowledge there have been no studies of noble metal nanotubes as label-free sensors. In this paper we demonstrate the high potential of vertically aligned gold nanotube arrays for label-free bioanalytical sensing. Bulk sensitivity of both the inside and outside walls of the nanotubes is determined, and interfacial sensitivity to the response induced by biomolecular binding reactions is studied. The results are compared with finite element simulations and explained by field distributions associated with the plasmonic resonance peculiar to the nanotube geometry.

Recently, we presented a method, schematically illustrated in Figure 1, to fabricate arrays of gold nanotubes by electrodeposition of gold around polypyrrole nanorods in a thin anodic alumina (AAO) template.[32] First, a nanoporous AAO template is fabricated on a substrate by anodizing an aluminum thin film on a thin gold under-layer. Then, polypyrrole is deposited into the AAO pores (Figure 1A) by electropolymerization. The AAO pores are then chemically etched using NaOH, creating shells around the polypyrrole nanorods (Figure 1B). Gold is then electrodeposited into the shells (Figure 1C). At the next stage, the polypyrrole is removed by plasma etching (Figure 1D). An outer shell is then formed by chemical etching as before (Figure 1E). If the etch is continued, the AAO matrix is completely removed (Figure 1F) to reveal freestanding arrays of gold nanotubes attached to the substrate (Figure 1G).

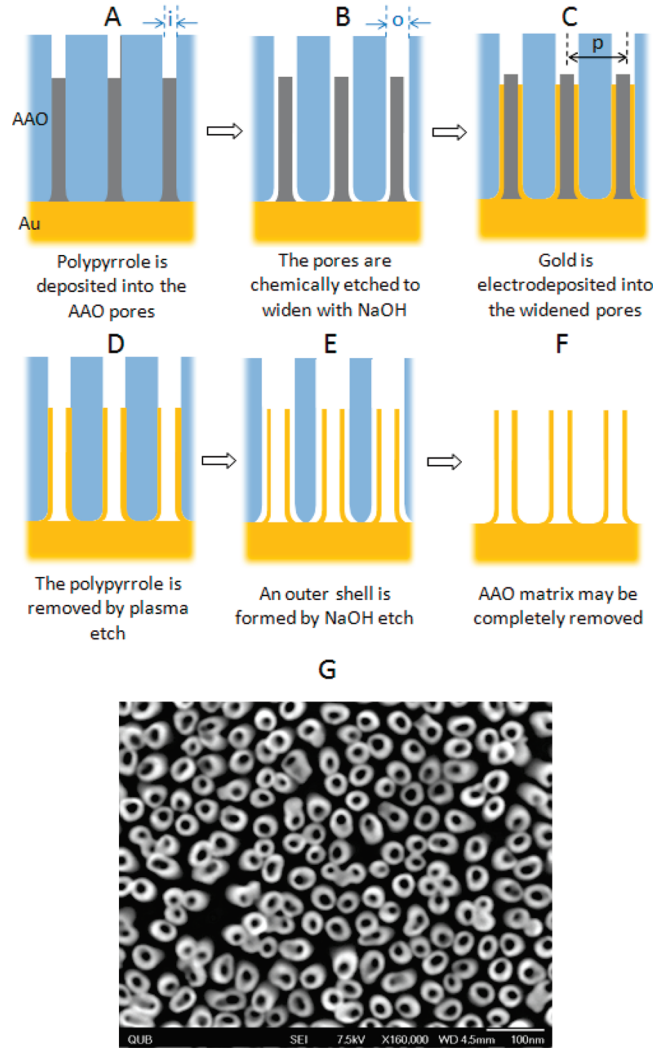

Figure 1. Summary of the fabrication process for gold nanotube arrays and SEM image of the resulting structure. The sample dimensions inner diameter (i), outer diameter (o), and pitch (p) are indicated.

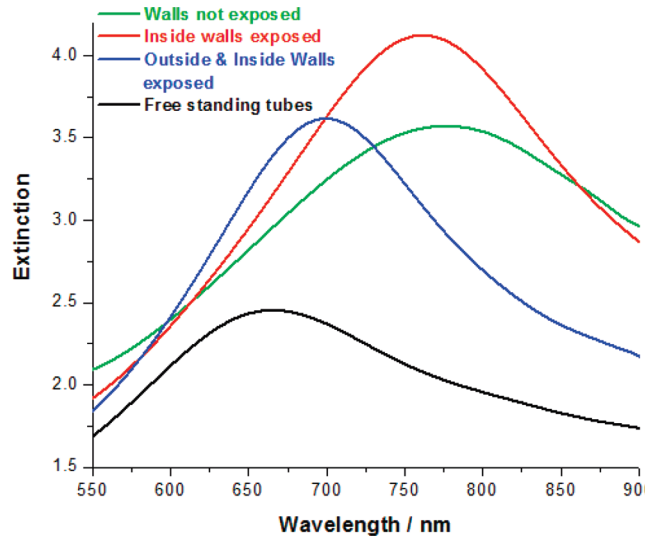

Figure 2. Extinction spectra obtained in water for a gold nanotube sample at different stages during the fabrication. The sample has average tube dimensions of length = 120 nm, inner diameter *i* = 22 nm, and outer diameter *o* = 44 nm and *p* = 55 nm. Angle of incidence θ = 0°.

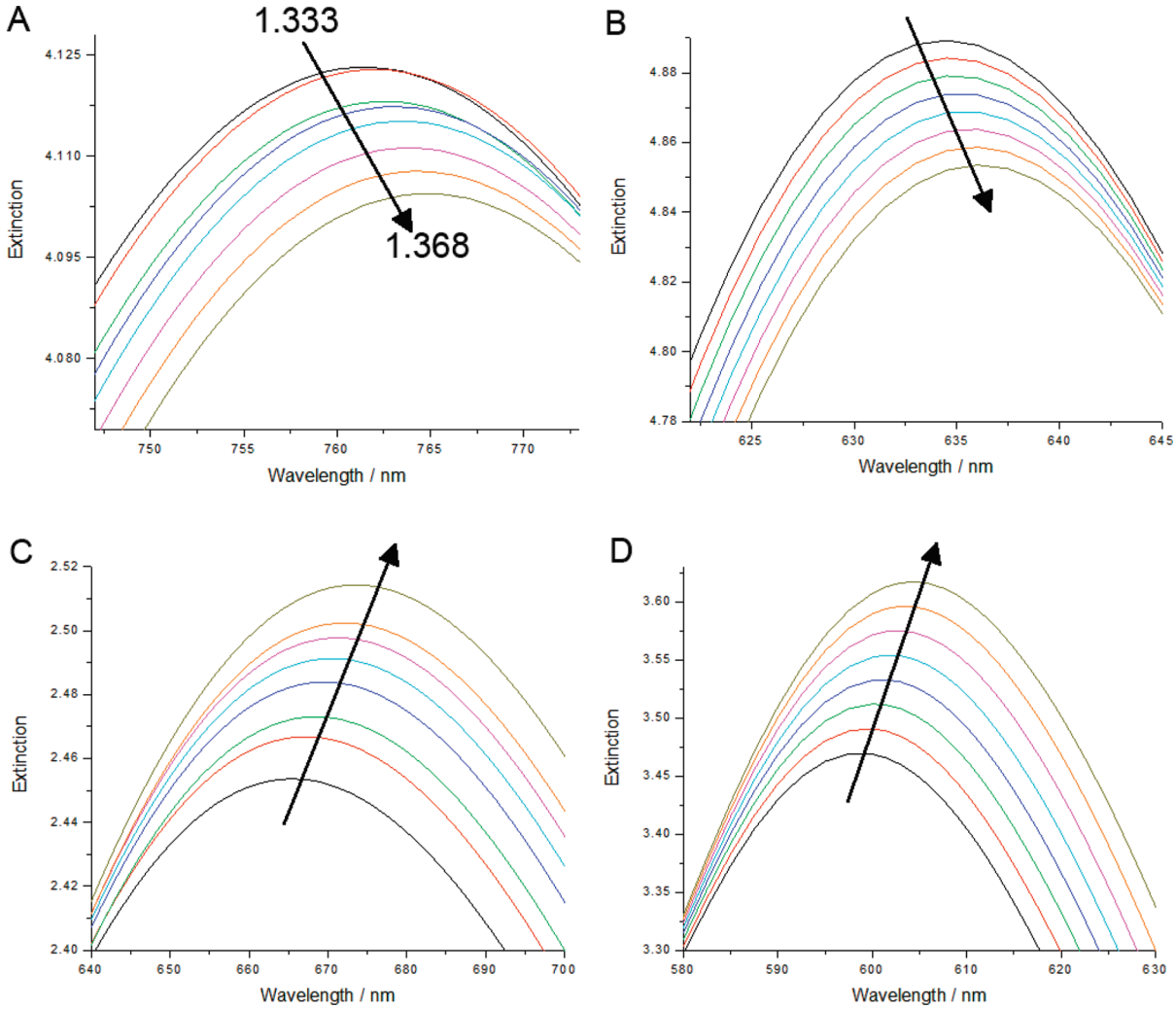

Figure 3. Extinction spectra for different concentrations of glycerol in water (0−40 wt %/RI = 1.333−1.368). (A) Experimentally acquired from a sample with only inside walls exposed and (B) the respective FEM simulated spectra, (C) Experimentally acquired for both inside and outside walls exposed and (D) the respective FEM simulated spectra. The arrows indicate the direction of peak shift with increasing refractive index. θ = 0°.

RESULTS AND DISCUSSION

Figure 2 shows optical extinction spectra acquired from transmission measurements at normal incidence with the samples immersed in water. Using normal incidence radiation significantly simplifies the experimental setup in terms of biosensing applications as it renders the use of specific angles and polarized light unnecessary. Longitudinal plasmonic[23,24] modes will only be observed for angle of incidence (θ) other than zero, and hence in the spectra presented the plasmonic mode observed is a transverse one. The trace labeled "walls not exposed" (green) corresponds with the schematic in Figure 1C and shows an extinction peak at approximately 775 nm corresponding to a transverse plasmonic resonance. The spectrum labeled "inside walls exposed" (red) was acquired following removal of the polypyrrole by plasma etching in a 3:1 argon−oxygen atmosphere at 15 W for 10 min (schematic Figure 1D). From this treatment the extinction peak was seen to increase, sharpen, and blue-shift slightly. The blue-shift is in agreement with the fact that the RI inside the gold nanotubes decreases from around 1.45 for the polypyrrole to 1.333 for water.[33] It is known that post annealing samples results in an increase in the gold's mean-free path leading to a reduction of the imaginary part of the permittivity of Au.[34,35] As the sample heats slightly during plasma etching this transition could also be partially attributable to this effect. The "outside and inside walls exposed" trace (blue) was acquired following chemical etching of the alumina in 0.03 M sodium hydroxide (NaOH) for 30 s to create an outer shell around the tubes. This structure corresponds with that illustrated in Figure 1E. The extinction peak decreases and blue shifts by around 65 nm following the partial alumina etch because of the decrease in the effective RI of the water-filled shell. As seen in the trace "free-standing tubes", the peak is further suppressed, broadened, and blue-shifted following the removal of all of the alumina (depicted in Figure 1F).

The nanotube plasmonic resonance sensitivity was then investigated with respect to changes in RI of the surrounding medium through immersion in different concentrations of glycerol dissolved in water (0−40 wt %). The RI of each solution was verified using an Abbe refractometer.

Spectra obtained for inside walls exposed and inside and outside walls exposed are shown in Figure 3 panels A and C, respectively. Also shown for comparison are spectra generated using finite element modeling (FEM) software Comsol Multiphysics 3.5a (RF Module). The models assume a square lattice arrangement with typical parameters (pitch, 55 nm; length, 100 nm; inner diameter, 22 nm; outer diameter, 44 nm; and gold permittivity with a reduced mean free path of 3 nm).[34,35]

The simulated spectra of this complex system are not meant to be a fit to data but are for qualitative comparison with observations when the refractive index changes. Differences between the real material constants and model are expected leading to deviations of the exact position of the resonances in the modeled and experimental spectra. The resonance behavior in response to the refractive index change of the surroundings is completely reproduced by the model.

In agreement with the simulations, the experimental spectra reveal that both the inside and the outside of the nanotubes are sensitive to RI changes. It was seen earlier (Figure 2) that only exposing the nanotube inside walls resulted in a blue-shift of the extinction peak and an increase in extinction related to the reduced refractive index inside the nanotubes. These trends are confirmed on increasing the refractive index (Figure 3A) resulting in a red-shift and reduction of the extinction peak and are in qualitative agreement with simulations (Figure 3B). When both inside and outside walls are exposed (Figure 3C,D), again, the extinction peak red-shifts with RI, but this time the extinction increases according to both experiment and simulation.

The dependence of peak extinction on refractive index is graphically illustrated in Figure 4, revealing linearity in both cases, which is consistent with FEM results. To evaluate the bulk sensitivity of the nanostructures the extinction peak shift ($\Delta\lambda_{peak}$) was plotted against the change in RI (Figure 5). The bulk sensitivity is defined as $m = \Delta\lambda_{peak}/\Delta RI$ and could be determined from linear fits to the experimental data points.

The figure shows that before the tube walls are exposed the samples are essentially insensitive to the changes in RI of the solutions. This behavior suggests that the electromagnetic field of the nanotubes' plasmonic excitation is confined within the matrix. After the inside walls are exposed the structure becomes sensitive to changes in RI of the bulk medium with a sensitivity of 98 nm/RIU (refractive index units). With both inside and outside walls being exposed, the bulk

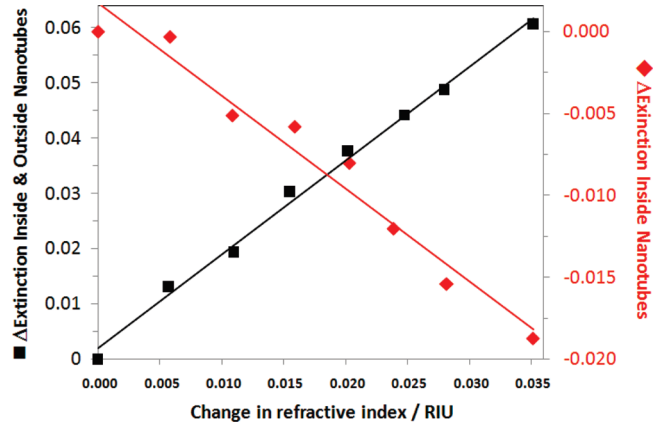

Figure 4. Change in extinction at the peak wavelength as a result of immersion in different concentrations of glycerol in water (0−40 wt %) for a sample with only inside walls of nanotubes exposed and for a sample with both inside and outside walls exposed. The solid lines are linear fits to the data points. θ = 0°.

sensitivity increased to 225 nm/RIU. Thus the exposure of both inside and outside walls increases the sensitivity of the transducer.

A sensitivity of 225 nm/RIU for the nanotube arrays is competitive with that of other gold-based LSPR structures with resonances around 650 nm, and it is expected that it can be further improved by tuning the plasmonic nanotube resonance toward the red region of the wavelength range.[10,36,37] Our system, however, provides additional advantages such as broad spectral tuneability and a large effective surface area.

Numerical modeling was also used to gain an insight into the underlying nature of the sensitivity of the nanotube surfaces. The electromagnetic field distribution for a free-standing nanotube in an array excited by a plane wave at normal incidence is shown in Figure 6. The field enhancement along the outer tube walls in Figure 6A supports the experimental observations which showed that the exposure of the outside walls of the nanotube yields high sensitivity. Near the

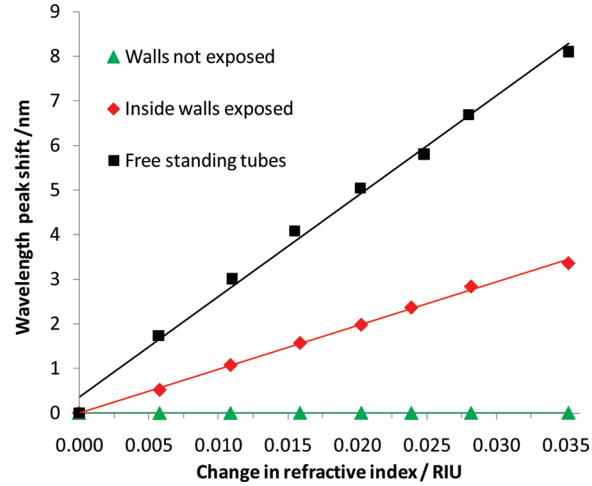

Figure 5. Sensitivity of the wavelength of the extinction peak to changes in refractive index by immersion in different concentrations of glycerol in water (0−40 wt %) for the same structure at different stages of the fabrication process. θ = 0°.

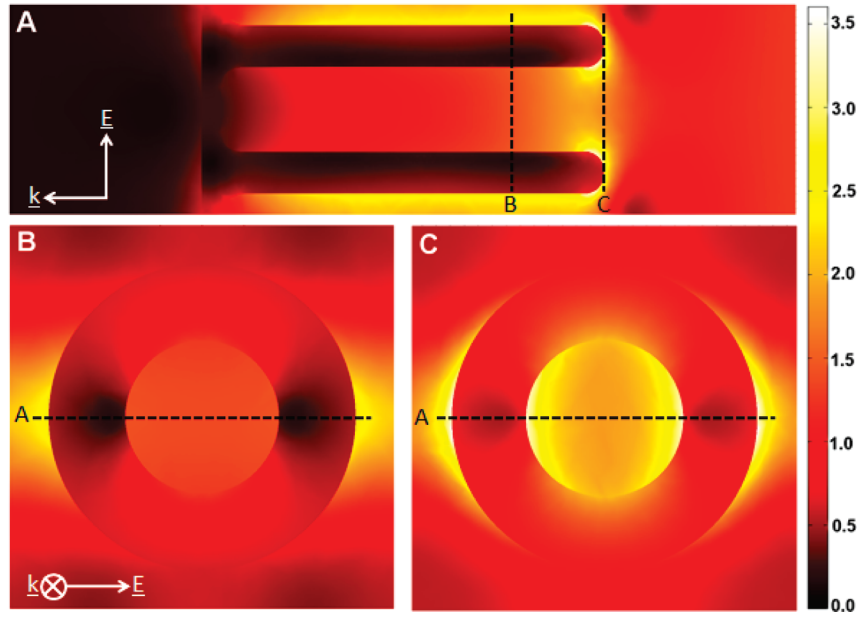

Figure 6. The FEM simulated distributions of the norm of electric field in free-standing gold nanotube arrays at the wavelength at which extinction is a maximum. Cross-section A shows the distribution of the field along the length of the nanotubes, image B shows the distribution for a cross-section at 25 nm from the rim of the nanotube, and image C is the distribution at the rim itself. The model assumed a pitch of 55 nm; nanotube length, 100 nm; inner diameter, 22 nm; and outer diameter, 44 nm. θ = 0°.

rim of the nanotube the field is significant both inside and outside the tube.

Finally, the ability of free-standing nanotubes to detect biomolecular binding was evaluated through the binding of NeutrAvidin protein to the tubes. For this experiment the sample was placed in a flow cell and the plasmonic resonance was monitored in real-time *via* the centroid of the peak (wavelength at the center of mass).[15] The flow cell was first filled with buffer followed by the addition of 10 μg/mL NeutrAvidin (167nM) at the time 0 min (Figure 7). This resulted in a monotonic binding curve that saturates at a remarkably high shift of around 16 nm. Indeed, this shift

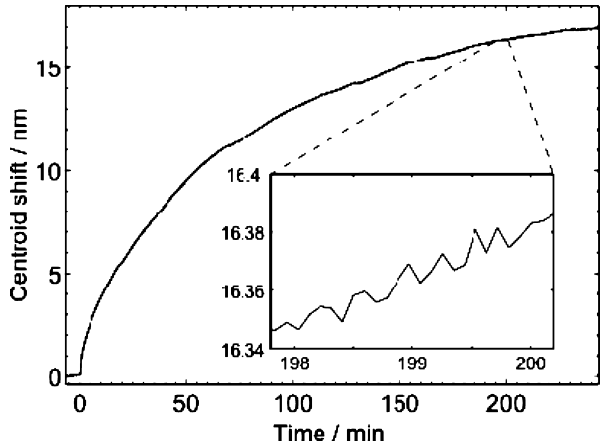

Figure 7. Temporal variation in the centroid position during adsorption of 10 μg/mL NeutrAvidin (added at 0 min) to a free-standing gold nanotube array. The inset shows a zoomed section of the graph and illustrates both the noise level (~1 × 10^{-2} nm) and the temporal resolution (~5 s) of the measurement. θ = 0°.

should be considered large even compared with those induced by protein adsorption on nanoplasmonic sensors with higher bulk sensitivity than the presented structure.[14] It is also interesting to note that the protein uptake is significantly slower than that expected under stagnant conditions at this concentration. This could be due to protein-binding to the rims of the tubes slowing down the diffusion of molecules to the insides of the tubes. This, combined with the large differences in field strength over the nanostructure's surface could enable size selective biomolecular filtering.

In summary, we have successfully fabricated vertically aligned gold nanotube arrays on glass substrates using a self-assembly technique and explored the bulk and interfacial sensitivity of their optical properties to refractive index variations. The free-standing tubes displayed very competitive sensitivities as compared with other LSPR-based nanoplasmonic structures and exhibited a very large peak shift and signal-to-noise ratio in biomolecular binding experiments using the protein NeutrAvidin.

Apart from the importance and applicability of high performance RI sensors in general, arrays of free-standing plasmonic nanotubes have the potential to be used to penetrate cells without interfering with their survival.[37] Combined with recent developments where LSPR sensing from microscale areas has been achieved without loss in signal-to-noise ratio compared with macroscale sensing,[38] the fact that the field strength is highest at the rim of the nanotubes could enable a unique means of probing cell interiors down to the single cell level.

METHODS

Substrate-Bound Gold Nanotube Array Fabrication Process. The samples were prepared through a multistage process thoroughly described previously.[32] First, 8 nm tantalum pentoxide (Ta_2O_5), 5 nm gold (for subsequent electrodepositions), and 400 nm aluminum films were magnetron-sputter deposited onto glass substrates in an ambient pressure of 5 μbar. The Ta_2O_5 adhesion layer was sputtered in a 20% oxygen/80% argon mixture, while pure argon was used for the others. Anodization of the aluminum was performed in 0.3 M sulfuric acid (~1 °C) at constant voltage using a platinum counterelectrode. Following anodization the nanoporous alumina templates were etched in 30 mM NaOH to remove the barrier layer from the base of the resulting pores. The duration of this etch also determines the diameter of the subsequently deposited sacrificial polymer wires.

Polypyrrole (PPy) was deposited into the AAO template using a standard three-electrode cell at an electropolymerization voltage of +1.5 V against a platinum reference wire. The electrolyte was an acetonitrile solution containing 0.5 M pyrrole monomer and 0.3 M tetraethylammonium-*p*-toluene sulfonate.[39] The AAO pores surrounding the PPy nanowires were widened using a 30 mM NaOH etch and gold was electrodeposited *versus* a saturated calomel electrode into the resulting shell from a sodium thiosulfate−sulfite bath.[40] The PPy nanowires were removed by reactive plasma etching in a 3:1 argon−oxygen atmosphere at low power (15 W). The AAO template may also be removed using NaOH etching to reveal free-standing gold nanotubes.

Optical Characterization System. To characterize the RI sensing capability of the samples, they were mounted in a transparent flow cell arrangement and optical transmission spectra were acquired *via* a 1.5 mm diameter fiber bundle placed directly behind the sample. The fiber is coupled to a spectrograph (Andor, Shamrock 303i) and CCD camera (Andor, Newton) under computer control. The optical response was kinetically recorded as the samples were immersed in different concentrations of glycerol (Sigma-Aldrich) dissolved in water (0−40 wt %). The RI of each solution was verified using an Abbe refractometer. Analysis of nanotube dimensions was performed using a JEOL 6500F scanning electron microscope.

FEM. Finite element simulations of the near and far-field optical response were carried out using Comsol Multiphysics 3.5a (RF Module) software.

Acknowledgment. The authors acknowledge the Engineering and Physical Sciences Research Council (UK) for financial support. The authors acknowledge the Engineering and Physical Sciences Research Council (UK), the Swedish Research Council and the Swedish Strategic Research Foundation for financial support.

REFERENCES AND NOTES

1. Sanders, G. H. W.; Manz, A. Chip-Based Microsystems for Genomic and Proteomic Analysis. *Trends Anal. Chem.* **2000**, *19*, 364–378.
2. SolinasToldo, S.; Lampel, S.; Stilgenbauer, S.; Nickolenko, J.; Benner, A.; Dohner, H.; Cremer, T.; Lichter, P. Matrix-Based Comparative Genomic Hybridization: Biochips To Screen for Genomic Imbalances. *Genes Chromosomes Cancer* **1997**, *20*, 399–407.
3. Michalet, X.; Kapanidis, A. N.; Laurence, T.; Pinaud, F.; Doose, S.; Pflughoefft, M.; Weiss, S. The Power and Prospects of Fluorescence Microscopies and Spectroscopies. *Annu. Rev. Biophys. Biomol. Struct.* **2003**, *32*, 161–182.
4. Webb, S. E. D.; Roberts, S. K.; Needham, S. R.; Tynan, C. J.; Rolfe, D. J.; Winn, M. D.; Clarke, D. T.; Barraclough, R.; Martin-Fernandez, M. L. Single-Molecule Imaging and Fluorescence Lifetime Imaging Microscopy Show Different Structures for High- and Low-Affinity Epidermal Growth Factor Receptors in A431 Cells. *Biophys. J.* **2008**, *94*, 803–819.
5. Janshoff, A.; Galla, H. J.; Steinem, C. Piezoelectric Mass-Sensing Devices as Biosensors—An Alternative to Optical Biosensors. *Angew. Chem.—Int. Ed.* **2000**, *39*, 4004–4032.
6. Rodahl, M.; Hook, F.; Krozer, A.; Brzezinski, P.; Kasemo, B. Quartz Crystal Microbalance Setup for Frequency and Q-Factor Measurements in Gaseous and Liquid Environments. *Rev. Sci. Instrum.* **1995**, *66*, 3924–3930.
7. Zheng, G. F.; Patolsky, F.; Cui, Y.; Wang, W. U.; Lieber, C. M. Multiplexed Electrical Detection of Cancer Markers with Nanowire Sensor Arrays. *Nat. Biotechnol.* **2005**, *23*, 1294–1301.
8. Liedberg, B.; Nylander, C.; Lundstrom, I. Biosensing with Surface Plasmon Resonance—How It All Started. *Sens. Actuators* **1983**, *4*, 299–304.
9. Kretschmann, E.; Raether, H. Radiative Decay of Non Radiative Surface Plasmons Excited By Light. *Z. Naturforsch. A* **1968**, *23*, 2135.
10. Anker, J. N.; Paige Hall, W.; Lyandres, O.; Shah, N. C.; Zhao, J.; Van Duyne, R. P. Biosensing with Plasmonic Nanosensors. *Nat. Mater.* **2008**, *7*, 442–453.
11. Jonsson, M. P.; Dahlin, A. B.; Jönsson, P.; Höök, F. Nanoplasmonic Biosensing with Focus on Short-Range Ordered Nanoholes in Thin Metal Films (Review). *Biointerphases* **2008**, *3*, FD30–FD40.
12. Brian, B.; Sepulveda, B.; Alaverdyan, Y.; Lechuga, L. M.; Kall, M. Sensitivity Enhancement of Nanoplasmonic Sensors in Low Refractive Index Substrates. *Opt. Express* **2009**, *17*, 2015–2023.
13. Dmitriev, A.; Hagglund, C.; Chen, S.; Fredriksson, H.; Pakizeh, T.; Kall, M.; Sutherland, D. S. Enhanced Nanoplasmonic Optical Sensors with Reduced Substrate Effect. *Nano Lett.* **2008**, *8*, 3893–3898.
14. Larsson, E. M.; Alegret, J.; Kall, M.; Sutherland, D. S. Sensing Characteristics of NIR Localized Surface Plasmon Resonances in Gold Nanorings for Application as Ultrasensitive Biosensors. *Nano Lett.* **2007**, *7*, 1256–1263.
15. Dahlin, A. B.; Tegenfeldt, J. O.; Höök, F. Improving the Instrumental Resolution of Sensors Based on Localized Surface Plasmon Resonance. *Anal. Chem.* **2006**, *78*, 4416–4423.
16. Hulteen, J. C.; van Duyne, R. P. Nanosphere Lithography: A Materials General Fabrication Process for Periodic Particle Array Surfaces. *J. Vac. Sci. Technol., A* **1995**, *13*, 1553–1558.
17. Hanarp, P.; Sutherland, D. S.; Gold, J.; Kasemo, B. Control of Nanoparticle Film Structure for Colloidal Lithography. *Colloid. Surf., A* **2003**, *214*, 23–36.
18. Fredriksson, H.; Alaverdyan, Y.; Dmitriev, A.; Langhammer, C.; Sutherland, D. S.; Zaech, M.; Kasemo, B. Hole-Mask Colloidal Lithography. *Adv. Mater.* **2007**, *19*, 4297–4302.
19. Stewart, M. E.; Mack, N. H.; Malyarchuk, V.; Soares, J.; Lee, T. W.; Gray, S. K.; Nuzzo, R. G.; Rogers, J. A. P. Quantitative Multispectral Biosensing and 1D Imaging Using Quasi-3D Plasmonic Crystals. *Natl. Acad. Sci. U.S.A.* **2006**, *103*, 17143–17148.
20. Evans, P. R.; Hendren, W. R.; Atkinson, R.; Wurtz, G. A.; Dickson, W.; Zayats, A. V.; Pollard, R. J. Growth and Properties of Gold and Nickel Nanorods in Thin Film Alumina. *Nanotechnology* **2006**, *17*, 5746.
21. Evans, P. R.; Hendren, W. R.; Atkinson, R.; Pollard, R. J. Optical Transmission Measurements of Silver, Silver−Gold Alloy, and Silver−Gold Segmented Nanorods in Thin Film Alumina. *Nanotechnology* **2008**, *19*, 5708.
22. Evans, P. R.; Hendren, W. R.; Atkinson, R.; Pollard, R. J. Nickel-Coated Gold-Core Nanorods Produced by Template Assisted Electrodeposition. *J. Electrochem. Soc.* **2007**, *154*, K79–K82.
23. Kabashin, A. V.; Evans, P.; Pastkovsky, S.; Hendren, W.; Wurtz, G. A.; Atkinson, R.; Pollard, R.; Podolskiy, V. A.; Zayats, A. V. Plasmonic Nanorod Metamaterials for Biosensing. *Nat. Mater.* **2009**, *8*, 867–871.
24. Evans, P. R.; Wurtz, G. A.; O'Connor, D.; Atkinson, R.; Hendren, W.; Dickson, W.; Pollard, R. J.; Zayats, A. V. Plasmonic Core/Shell Nanorod Arrays: Subattoliter Controlled Geometry and Tunable Optical Properties. *J. Phys. Chem. C* **2007**, *111*, 12522–12527.
25. Englebienne, P. Use of Colloidal Gold Surface Plasmon Resonance Peak Shift to Infer Affinity Constants From the Interactions between Protein Antigens and Antibodies

Specific for Single or Multiple Epitopes. *Analyst* **1998**, *123*, 1599–1603.
26. Chen, C.; Cheng, S.; Chau, L.; Wang, C. Sensing Capability of the Localized Surface Plasmon Resonance of Gold Nanorods. *Biosens. Bioelectron.* **2007**, *22*, 926–932.
27. Okamoto, T.; Yamaguchi, I.; Kobayashi, T. Local Plasmon Sensor with Gold Colloid Monolayers Deposited Upon Glass Substrates. *Opt. Lett.* **2000**, *25*, 372–374.
28. Lee, S.; Mayer, K. M.; Hafner, J. H. Improved Localized Surface Plasmon Resonance Immunoassay with Gold Bipyramid Substrates. *Anal. Chem.* **2009**, *81*, 4450–4455.
29. Wang, H.; Brandl, D. W.; Le, F.; Nordlander, P.; Halas, N. J. Nanorice: A Hybrid Plasmonic Nanostructure. *Nano Lett.* **2006**, *6*, 827–832.
30. Lee, J.; Hasan, W.; Odom, T. W. Tuning the Thickness and Orientation of Single Au Pyramids for Improved Refractive Index Sensitivities. *J. Phys. Chem. C* **2009**, *113*, 2205–2207.
31. Grigorenko, A. N.; Gleeson, H. F.; Zhang, Y.; Roberts, N. W.; Sidorov, A. R.; Panteleev, A. A. Antisymmetric Plasmon Resonance in Coupled Gold Nanoparticles as a Sensitive Tool for Detection of Local Index of Refraction. *Appl. Phys. Lett.* **2006**, *88*, 124103.
32. Hendren, W. R.; Murphy, A.; Evans, P.; O'Connor, D.; Wurtz, G. A.; Zayats, A. V.; Atkinson, R.; Pollard, R. J. Fabrication and Optical Properties of Gold Nanotube Arrays. *J. Phys.: Condens. Matter* **2008**, *20*, 362203.
33. Kim, D. R.; Cha, W.; Paik, W. Ellipsometric Studies on Polypyrrole and Polyaniline. *Synth. Mater.* **1997**, *84*, 759–760.
34. Atkinson, R.; Hendren, W. R.; Wurtz, G. A.; Dickson, W.; Zayats, A. V.; Evans, P. R.; Pollard, R. J. Anisotropic Optical Properties of Arrays of Gold Nanorods Embedded in Alumina. *Phys. Rev. B* **2006**, *73*, 235402.
35. Pollard, R. J.; Murphy, A.; Hendren, W. R.; Evans, P. R.; Atkinson, R.; Wurtz, G. A.; Zayats, A. V.; Podolskiy, V. A. Optical Nonlocalities and Additional Waves in Epsilon-Near-Zero Metamaterials. *Phys. Rev. Lett.* **2009**, *102*, 127405.
36. Chen, H.; Kou, X.; Yang, Z.; Ni, W.; Wang, J. Shape- and Size-Dependent Refractive Index Sensitivity of Gold Nanoparticles. *Langmuir* **2008**, *24*, 5233–5237.
37. Miller, M. M.; Lazarides, A. A. Sensitivity of Metal Nanoparticle Surface Plasmon Resonance to the Dielectric Environment. *J. Phys. Chem. B* **2005**, *109*, 21556–21565.
38. Dahlin, A. B.; Chen, S.; Jonsson, M. P.; Gunnarsson, L.; Kall, M.; Höök, F. High-Resolution Microspectroscopy of Plasmonic Nanostructures for Miniaturized Biosensing. *Anal. Chem.* **2009**, *81*, 6572–6580.
39. Rapta, P.; Neudeck, A.; Petr, A.; Dunsch, L. *In Situ* EPR/UV−vis Spectroelectrochemistry of Polypyrrole Redox Cycling. *J. Chem. Soc., Faraday Trans.* **1998**, *94*, 3625–3630.
40. Liew, M. J.; Roy, S.; Scott, K. Development of a Nontoxic Electrolyte for Soft Gold Electrodeposition: An Overview of Work at University of Newcastle Upon Tyne. *Green Chem.* **2003**, *5*, 376.